ChemInform Abstract: Evolution of Actinyl Peroxide Clusters U 28 in Dilute Electrolyte Solution: Exploring the Transition from Simple Ions to Macroionic Assemblies.

ARTICLE *in* CHEMISTRY - A EUROPEAN JOURNAL · MAY 2014

Impact Factor: 5.73 · DOI: 10.1002/chem.201303266 · Source: PubMed

4 AUTHORS, INCLUDING:

Dong Li
Carnegie Mellon University
22 PUBLICATIONS **456** CITATIONS
SEE PROFILE

May Nyman
Oregon State University
151 PUBLICATIONS **2,289** CITATIONS
SEE PROFILE

Tianbo Liu
University of Akron
145 PUBLICATIONS **3,948** CITATIONS
SEE PROFILE

ChemPubSoc Europe

DOI: 10.1002/chem.201303266

CHEMISTRY
A European Journal
Full Paper

Polyoxometalates

Evolution of Actinyl Peroxide Clusters U_{28} in Dilute Electrolyte Solution: Exploring the Transition from Simple Ions to Macroionic Assemblies

Dong Li,[a] Silas Simotwo,[a] May Nyman,*[b] and Tianbo Liu*[a, c]

Abstract: Actinyl peroxide clusters, a unique class of uranyl-containing nanoclusters discovered in recent years, are crucial intermediates between the $(UO_2)^{2+}$ aqua-ion monomer and bulk uranyl minerals. Herein, two actinyl polyoxometalate nanoclusters of $Cs_{15}[(Ta(O_2)_4)Cs_4K_{12}(UO_2(O_2)_{1.5})_{28}]\cdot 20\,H_2O$ ($CsKU_{28}$) and $Na_6K_9[(Ta(O_2)_4)Rb_4Na_{12}(UO_2(O_2)_{1.5})_{28}]\cdot 20\,H_2O$ ($RbNaU_{28}$) were synthesized by incorporating a central $Ta(O_2)_4^{3-}$ anion that templates a hollow shell of 28 uranyl peroxide polyhedra. When dissolved in aqueous solutions with additional electrolytes, those 1.8 nm-size macroanions self-assembled into spherical, hollow, blackberry-type supramolecular structures, as was characterized by laser-light scattering (LLS) and TEM techniques. These clusters are the smallest macroions reported to date that form blackberry structures in solution, therefore, can be treated as valuable models for investigating the transition from simple ions to macroions. Kinetic studies showed an unusually long lag phase in the initial self-assembly process, which is followed by a rapid formation of the blackberry structures in solution. The small cluster size and high surface-charge density are essential in regulating the supramolecular structure formation, as was shown from the high activation energy barrier of 51.2 ± 2 kJ mol^{-1}. Different countercations were introduced into the system to investigate the effect of ion binding to the length of the lag phase. The current research provides yet another scale of self-assembly of uranyl peroxide complexes in aqueous media.

Introduction

Soluble macroions with a size of 2 to 6 nm in diameter behave quite differently from simple ions or colloidal particles.[1] They tend to self-associate when carrying moderate charges in polar solvents, followed by slow self-assembly into stable, hollow, spherical, blackberry-type supramolecular structures in solution, driven by the counterion-mediated attraction and hydrogen bonding.[2] Previous investigations have shown that this is a general phenomenon for both macrocations and macroanions.[3] The size disparity between large macroions and small counterions (ca. 10:1), which is much smaller than that in colloidal systems (ca. 1000:1), is critical for their unique solution behaviors. In this case, counterions can no longer be treated as point charges, that is, the effect of hydrated counterion size needs to be considered in dealing with the macroion/counterion interaction.[4] Ion pairing and the consequent counterion-mediated attraction may be enhanced under this circumstance even for monovalent counterions.[5] Herein, we have the opportunity to formulate new questions: What is the lower size limit of macroions that will assemble into blackberry structures? How do the macroions behave when they approach the sizes of simple ions? Is there any difference in the behavior of small macroions versus large macroions during blackberry assembly? Seeking these answers would greatly improve our understanding of the fundamentals of macroionic solutions and thus provide valuable insight to other colloidal or biological systems.[6] To date, the smallest macroanion with which we have been able to document blackberry assembly is $\{Cu_{20}P_8W_{48}\}$, a nanowheel with dimensions of approximately $2.2\times 2.2\times 1.1$ nm^3.[7]

Recent developments on the uranyl peroxide clusters present new scientific opportunities. The physical and chemical state of uranyl nanomaterials in the biosphere has always been one of the primary public concerns when considering using nuclear energy in the future, or remediating nuclear wastes of the past.[8] How to effectively track, transport, remediate, sequester and separate radionuclides is of practical importance, and obtaining fundamental knowledge of the radionuclides' behavior in aqueous environments is crucial.[9] Recent discoveries of actinyl polyoxometalate nanoclusters offer the opportunity to better understand the evolution of uranyl ion $(UO_2)^{2+}$ in solution, which is the foundation of uranyl chemistry.[10] Each uranyl ion can coordinate up to three peroxide ligands in

[a] Dr. D. Li, S. Simotwo, Prof. Dr. T. Liu
Department of Chemistry, Lehigh University
Bethlehem, Pennsylvania 18015 (USA)

[b] Prof. Dr. M. Nyman
Department of Chemistry, Oregon State University
Corvallis, Oregon 97331 (USA)
E-mail: may.nyman@oregonstate.edu

[c] Prof. Dr. T. Liu
Department of Polymer Science, The University of Akron
Akron, Ohio 44325 (USA)
E-mail: tliu@uakron.edu

Supporting information for this article is available on the WWW under http://dx.doi.org/10.1002/chem.201303266.

a bidentate fashion to form a bipyramidal polyhedra. These further self-assemble into rings, and then clusters,[11] in which the curvature is driven by the "inherently bent" UO_2-O_2-UO_2 dihedral angle (ca. 153° experimental; ca. 144° calculated) that is stabilized by molecular-orbital interactions in the bent configuration.[12] To date, about 40 actinyl nanoclusters with different sizes and geometries have been reported by Burns' group.[13] These structurally well-defined clusters are intermediate in size between $(UO_2)^{2+}$ monomers and bulk uranyl peroxide minerals (such as studtite) of infinite length scales. It has been suggested that actinyl peroxide clusters could naturally form in the storage pools of the nuclear power plants, in which uranium oxide fuel rods are in contact with water, and peroxide is abundant, produced by α-hydrolysis of water.[8a,14] The capsules normally carry a large negative charge that is mitigated by encapsulated and templating cations.[12] Their solution behaviors are unique and deserve in-depth investigation.[15] To date, there have been limited investigations on these actinyl clusters in dilute condition for an extended time scale.

Two actinyl peroxide clusters $Cs_{15}[(Ta(O_2)_4)Cs_4K_{12}(UO_2(O_2)_{1.5})_{28}]\cdot 20H_2O$ (CsK**U$_{28}$**) and $Na_6K_9[(Ta(O_2)_4)Rb_4Na_{12}(UO_2(O_2)_{1.5})_{28}]\cdot 20H_2O$ (RbNa**U$_{28}$**) were synthesized and investigated for this study. The structure of **U$_{28}$** was first reported by Burns et al. in 2005.[16] Synthetic methods were further developed by Nyman et al.,[17] and a series of new **U$_{28}$** clusters were obtained. The **U$_{28}$** clusters can be described as hollow capsules of 28 uranyl triperoxide monomers comprising a shell with twelve pentagonal rings (faces) and four hexagonal faces. In the center is an anion $(Ta(O_2)_4)^{3-}$ in the case of the current studies) with countercations (Na^+, K^+, Rb^+, and/or Cs^+) locating at both internal (templating) and external (charge balancing) the capsule. The Na^+ and K^+ reside under the pentagonal faces and Rb^+ and Cs^+ are found in the hexagonal faces,[17] self-selected by the ion size. These capsules show remarkable structural stability and fascinating ion-exchange properties in solution.[18] More importantly, the **U$_{28}$** cluster is a small actinyl cluster (less than 2 nm in diameter) with high surface-charge density. Therefore, it is of considerable interest from both fundamental science and practical point of view to investigate the solution behavior of the **U$_{28}$** clusters.

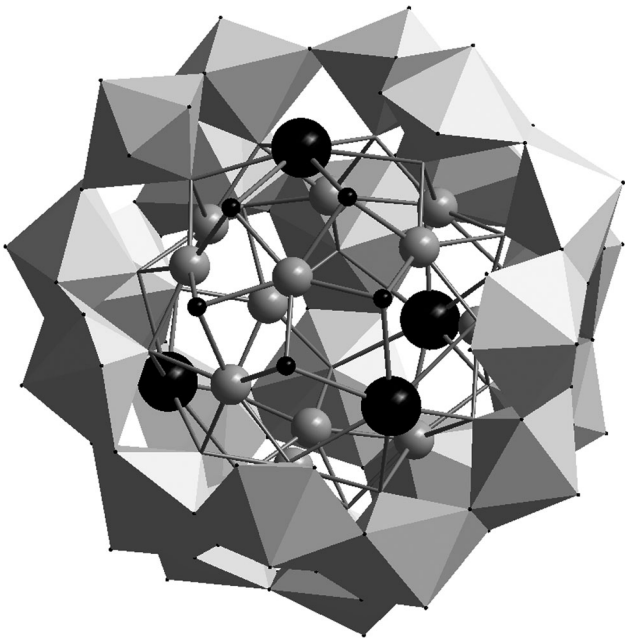

Scheme 1. View of **U$_{28}$** nanocluster. Gray polyhedra are $UO_2(O_2)_3$. Gray spheres are K^+ or Na^+ templating the pentagonal faces, large black spheres are Cs^+ or Rb^+ templating the hexagonal faces, and small black spheres are oxygen atoms. The central TaO_8 anions are eliminated for ease of viewing because of the front uranyl peroxide polyhedra.

Results and Discussion

Formation of the U$_{28}$ clusters

The **U$_{28}$** cluster represents one of the uranyl peroxide compounds that self-assemble from simple molecular uranyl species with well-defined size and structure; in other words, it is an energetically stable intermediate state between simple uranyl ion and bulk uranyl minerals. Good thermodynamic stability permits these clusters to persist for a long time in the absence of excess peroxide in solution.[14] **U$_{28}$** has an overall icosahedral geometry with a diameter of 1.77 nm, and is assembled from 28 identical uranyl peroxide polyhedra units, which encapsulate one central anion $[Ta(O_2)_4]^{3-}$ within the cluster under ambient conditions, as shown in Scheme 1. Both internal templating alkali cations and external charge-balancing cations affect the solution behavior of **U$_{28}$**, for example, the solubility.[18] Of particular note is the exchange behavior of the internal and external cations. The studies described herein show that this ion-exchange process affects their self-assembly behavior in solution. Because there is no OH groups attached to the U^{VI} center, this cluster does not deprotonate in aqueous solution as some polyoxomolybdates do. Furthermore, peroxide ligands and oxo ligand do not readily protonate. However, the alkaline self-buffering pH of the clusters indicated that there may be some exchange of internal cations with H_3O^+ upon dissolution. Nonetheless, the solubility and the potential self-assembly feature of these **U$_{28}$** clusters will be largely determined by the alkali countercations.

Self-assembly of U$_{28}$ clusters in solution

In aqueous solution, external counterions dissociate from the **U$_{28}$** cluster, whereas the internal cations might exchange with the external counterions and/or H_3O^+, resulting in increase of both solution pH and the net concentration of alkalis in solution that are not encapsulated. A recent report also shows the release and the exchange of the internal counterions of **U$_{28}$** at a high concentration (ca. 20 mg mL^{-1}) is possible.[18] The releasing of counterions should be even more rapid at lower **U$_{28}$** concentrations. Therefore, considering the small size of this cluster, its effective surface-charge density ρ_{eff} should be higher than previously studied giant POM macroions.[3a] One way to estimate the surface-charge density is to measure the solution conductivity. The conductance of a fresh 0.42 mg mL^{-1} (4.31×10^{-5} mol L^{-1}) RbNa**U$_{28}$** aqueous solution was measured

as 72 ± 3 μS, which is close to the calculated value of 86.0 μS by assuming that all the countercations (internal and external) were fully released from the clusters. Considering that the external counterions (6 Na^+ and 9 K^+) only contribute 42.0 μS, a large portion of the internal counterions should also be released into the solution. Therefore, the ρ_{eff} of RbNa**U$_{28}$** is expected to be higher than −15 charges/cluster, or $-0.24\ Cm^{-2}$. CsK**U$_{28}$** cannot be dissolved in deionized water due to the strong ionic interactions between Cs^+ ions and the **U$_{28}$** clusters. However, CsK**U$_{28}$** can be dissolved in KOH solution. The conductivity of a 0.50 mg mL^{-1} (4.31×10^{-5} mol L^{-1}) CsK**U$_{28}$** solution with 2.44×10^{-3} mol L^{-1} KOH is 536 μS, which also indicates a full release of external Cs^+ ions and partial release of the internal counterions (see the Supporting Information). Table 1 summarizes the calculated charge densities of the two **U$_{28}$** clusters and several other giant POM macroanions studied prior. At first glance, it is evident that even with only 15 external counterions being released; the charge density of **U$_{28}$** clusters is already high enough to suggest that self-assembly into blackberry structures is not possible in dilute aqueous solutions. In fact, the CsK**U$_{28}$** macroions do not self-assemble in aqueous solution at or below room temperature (20 °C), because there is no change in the scattered intensity from the static light scatting (SLS) measurements for months. However, introducing additional electrolytes to the system or raising solution temperature can trigger the self-assembly of **U$_{28}$** clusters in solution. This could be a result of thermodynamics (too many charges, therefore, electrostatic repulsion among **U$_{28}$** is too strong), kinetics (the energy barrier for oligomer formation is too high) or both. The effect of the ionic strength, ion type, and temperature will be elaborated in the following discussions.

As shown in Figure 1A, for a 0.50 mg mL^{-1} (4.31×10^{-5} mol L^{-1}) CsK**U$_{28}$** in 0.05 mol L^{-1} KOH solution at 30 °C, the scattered intensity recorded by SLS shows a sigmoidal increment with time. The initial bright yellow, clear solution and the low scattered intensity from SLS indicate that the **U$_{28}$** clusters were fully dissolved and homogenously distributed in solution. The increase of the scattered intensity from the same sample indicates the formation of larger assemblies, although with an unusual long lag period of about 41 ± 2 days at 30 °C. The scattered intensity reached a plateau after about 120 days, indicating that the formation of large assemblies approached equilibrium. Moreover, the R_h (hydrodynamic radius) of the assembled structures recorded at 90° scattering angle by DLS measurement gradually increased after the lag period and was finally stabilized at approximately 70 nm, as shown in Figure 1B. Similar trends were observed in solutions with different **U$_{28}$** concentrations and under different temperatures (Figures S2 and S3 in the Supporting Information). Samples with KOH concentration less than 0.05 mol L^{-1} showed no increase of scattered intensity for months even at 30 °C.

The shape factor of $\gamma=R_g/R_h$ indicates the morphology of the assemblies in solution. For example, $\gamma=0.77$ for a solid sphere, $\gamma=0.82$ for a random coil, and $\gamma\geq1.73$ for a cylinder. For blackberries, γ is always close to 1.0, because blackberries are vesicle-like spheres with almost all its mass distributed on the surface. However, in a 0.5 mg mL^{-1} CsK**U$_{28}$** sample solution at 40 °C, γ gradually decreased from 2.5 to 1.0, as shown in Figure 1C, indicating that instead of directly forming the blackberry structures, individual **U$_{28}$** clusters form some elongated flat disc-like intermediates, which continued to grow until they folded into hollow, spherical blackberry structures to lower the overall free energy. It has been shown in the {$Mo_{72}Fe_{30}$} system that the oligomer (dimer or trimer) formation is the critical step for the successful assembly of blackberries.[19a] However, the presence of dimer of larger oligomers is hard to detect due to their transient nature in solution, and it is only possible to resolve the dimer structure of {$Mo_{72}Fe_{30}$} under high ionic-strength condition.[19a,20] In the current **U$_{28}$** system, the two-step self-assembly process (from monomer to long-living intermediate structures and then to blackberries) is apparently distinctive from large polyoxometalate (POM) macroanions. In addition to this, our previous studies have shown that it is possible to tune the size of blackberries with the introduction of different monovalent or divalent counterions in the {$Mo_{72}Fe_{30}$} system. This size change is not due to the growth of oligomers but the enlargement of blackberries (it has been noticed that once the blackberries are formed in aqueous solution, their size normally remain the same throughout the whole self-assembly process and only the number of blackberries increases).[19b,21]

Table 1. Summary on the surface-charge density of **U$_{28}$** and several other POM clusters.

POM clusters	Total charge number	Diameter of the cluster [nm]	Charge density [C m^{-2}]	Self-assembly in dilute aqueous solutions
$Mo_{72}Fe_{30}$	$-4\approx-29$	2.5	$-0.04\approx-0.24$	yes
Mo_{154}	−15	3.6	−0.08	yes
$W_{48}P_8Cu_{20}$	−25	2.0	−0.21	yes
Mo_{132}	−42	2.9	−0.25	yes (at high concentration)
$Mo_{72}V_{30}$	−34	2.5	−0.28	no
Mo_{368}	−48	6.0×4.0	−0.38	no
$RbNaU_{28}$	−31[a]	1.78	$-0.50>\rho>-0.24$	yes (with electrolytes)
$CsKU_{28}$	−31[a]	1.78	$-0.50>\rho>-0.24$	yes (with electrolytes)

[a] This number includes both internal and external counterions.

The scattered intensities from the solutions containing higher CsK**U$_{28}$** concentrations (4.0 and 5.0 mg mL^{-1}) dropped in the initial several days (about seven days for 4.0 mg mL^{-1} solution and about 20 days for 5.0 mg mL^{-1} solution), then stabilized, and finally started to increase after 30 days, indicating that perhaps CsK**U$_{28}$** first dissolves as small oligomers in highly concentrated CsK**U$_{28}$** samples (Figure S2 in the Supporting Information). These observations show the differences between the **U$_{28}$** and giant POM clusters during the blackberry formation.

Spherical, vesicle-like structures formed in a 0.50 mg mL^{-1} RbNa**U$_{28}$** aqueous solution with 0.05 mol L^{-1} KOH were also revealed by TEM studies (Figure 2). These supramolecular assemblies were

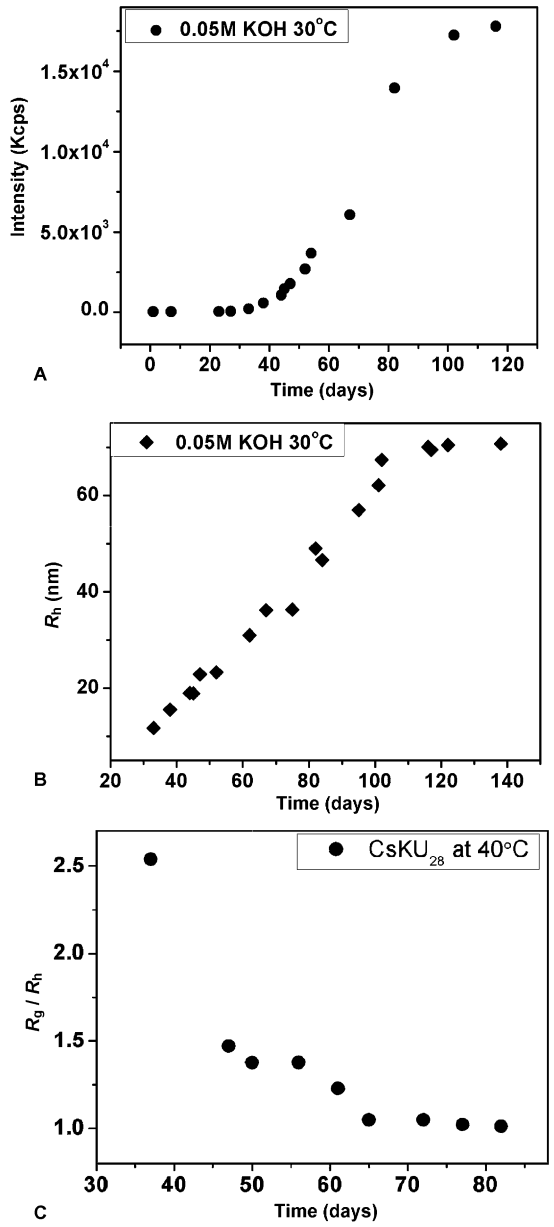

Figure 1. A) Total scattered intensity change with time for a 0.5 mg mL^{-1} (4.31×10^{-5} mol L^{-1}) Cs**KU_{28}** sample in the 0.05 mol L^{-1} KOH solution at 30 °C. B) The change of R_h for the same sample with time. C) The change of γ (the R_g/R_h ratio) with time for a 0.5 mg mL^{-1} Cs**KU_{28}** sample in 0.05 mol L^{-1} KOH solution at 40 °C.

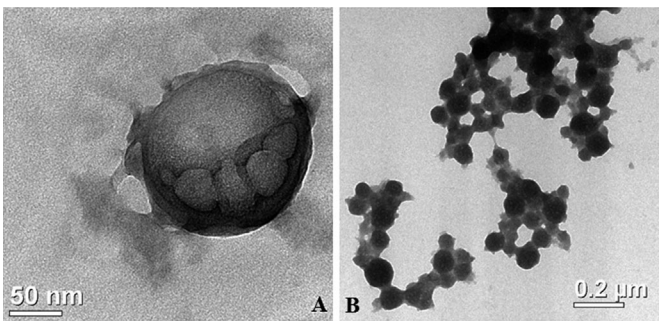

Figure 2. TEM images of the blackberry structures formed by **U_{28}** clusters in solution. A) 4.31×10^{-5} mol L^{-1} RbNa**U_{28}** in 0.05 mol L^{-1} KOH alkali solution, B) 4.31×10^{-5} mol L^{-1} Cs**KU_{28}** in 0.2 mol L^{-1} NH_4Cl solution.

broken under high vacuum condition due to their hollow nature, a clear indication that the **U_{28}** clusters indeed form blackberry-type structures in solution with additional electrolytes.

Temperature effect and the activation-energy barrier

Typically, the blackberry formation is a very slow process, due to the high energy barrier for the transition from single macroions to oligomers.[20] For example, it requires several months for the blackberry-formation process of a 0.50 mg mL^{-1} (3.1×10^{-5} mol L^{-1}) {$Mo_{72}Fe_{30}$} solution to reach equilibrium at room temperature.[19,20] The lag period of **U_{28}** in 0.05 mol L^{-1} KOH aqueous solution is about 61 days at room temperature, which decreases to 41 days at 30 °C and further reduces to 23 days at 40 °C. Again, from prior studies,[18] we know that the alkalis exit the cluster more rapidly with increasing temperature, which may correlate here with depopulation of these templating alkalis being a rate-determining step to blackberry formation. Time-resolved SLS measurements can be used to determine the initial "reaction" rates of oligomer formation in **U_{28}** electrolyte solutions at different temperatures. The inversed lag time ($1/\tau$) obtained from the SLS is used as the indication of the oligomer formation rate. By applying the Arrhenius equation [Eq. (1)]:

$$\ln(1/\tau) = -E_a/RT + \ln A \qquad (1)$$

in which E_a is the activation energy, R is the gas constant, T is the temperature in Kelvin, and A is the prefactor or the frequency factor, the activation energy of the oligomer formation can be calculated as 51.2 ± 2 kJ mol^{-1} (see Figure S4 in the Supporting Information), which is indeed very high, and quite close to some other macroionic systems, such as {$Mo_{72}Fe_{30}$} (65 ± 5 kJ mol^{-1}) in aqueous solution containing 0.17 mol L^{-1} NaI. The larger activation energy of oligomer formation in the {$Mo_{72}Fe_{30}$} system is probably due to the fact that its surface charges are localized on terminal OH groups, lowering the possibility of effective collisions between adjacent {$Mo_{72}Fe_{30}$} clusters. More importantly, the higher ionic strength of 0.17 mol L^{-1} NaI compared to 0.05 mol L^{-1} KOH tends to stabilize discrete macroanions more effectively, which in turn raises the activation energy for the transition from monomer to oligomer state.

Counterion and temperature effect on the lag phase during the blackberry-structure formation

The length of the lag period before the blackberry formation is sensitive to the hydrated counterion size, the counterion concentration, and temperature, as summarized in Table S1 in the Supporting Information. To investigate the cation effect, different chloride salts were introduced into the solution of Cs**KU_{28}**. For example, Li^+ ion cannot trigger the self-assembly of **U_{28}** even at a high LiCl concentration of 1.0 mol L^{-1}, probably due to its large hydration shell, which prevents the formation of

stable ion pairing. Meanwhile, NaCl and KCl can effectively reduce the length of the lag period; with K^+ has a stronger effect than Na^+ at the same ionic concentration. CsCl will immediately precipitate the $\mathbf{U_{28}}$ clusters even with a concentration <0.01 mol L^{-1}, implying that Cs^+ has a much stronger effect than K^+. Ammonium-type counterions can also affect the lag period of $\mathbf{U_{28}}$, especially for small NH_4^+ and tetramethylammonium (TMA^+). However, larger amphiphilic counterions, such as tetraethylammonium (TEA^+), tetrapropylammonium (TPA^+), and tetrabutylammonium (TBA^+) may interact with $\mathbf{U_{28}}$ in a different way, so that there is no clear lag phase during the self-assembly process, and the overall scattered intensity is also lower than those solutions with alkaline counterions at the same concentration when the self-assembly reached equilibrium, due to the fact that there is not excess alkali present, which is necessary to bridge the clusters in the blackberry structures (Figure S5 in the Supporting Information).

There are several other interesting observations related to the lag period. First, as shown in Figure 3, in a broad concentration range of added electrolytes, the change of the lag-

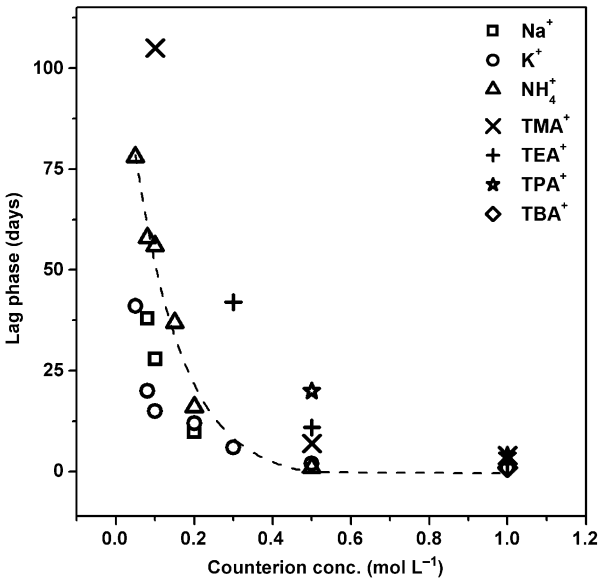

Figure 3. Influence of the addition of different electrolytes on the lag period of the blackberry-structure formation in 0.5 mg mL^{-1} Cs**K**$\mathbf{U_{28}}$ solution. Although the anion is chlorine in common, the cations were systematically varied. The dashed line is used to guide the eyes for the general trend of the change of the lag phase.

period time does not show a simple linear relationship with the electrolyte concentration but follows a roughly exponential decay with the salt concentration. At low counterion concentration range, there is one critical concentration above which the lag period is measurable, and the self-assembly process can proceed: for Na^+ 0.08 mol L^{-1}; for K^+ 0.05 mol L^{-1}; for NH_4^+ 0.05 mol L^{-1}; and for TMA^+ 0.10 mol L^{-1}. Second, the lag period is more sensitive to different counterions in lower concentration range. As shown in Figure 3, at 0.1 mol L^{-1} counterion concentration, the lag-period difference between K^+, NH_4^+, and TMA^+ is much more significant compared with that of 0.5 mol L^{-1}. Meanwhile, at higher counterion concentrations, the lag period is eliminated for most of the counterions around 1.0 mol L^{-1}. Counterions have duel effects on the lag phase: one is the specific ion-pairing formation, and the other is the increment of total ionic strength. Therefore, the current plot indicates at a lower concentration, the specific ion-pairing effect of different counterions is more critical; while at higher concentrations, the effect of total ionic strength increment takes over, and the difference between lag periods disappears.

The above-mentioned phenomena could be explained by the high charge density of $\mathbf{U_{28}}$ and its small size. The blackberry formation is a spontaneous, free-energy-favorable process with a huge activation-energy barrier between single macroanions and blackberries. In other words, the oligomeric state in the early nucleation step is unstable, and only when the oligomers' concentration reaches a critical value, the whole self-assembly process can move forward quickly, resulting in the unique sigmoidal curve of kinetics.[19,20] Therefore, the elongated lag period (much longer than the normal POM macroions) indicates that there is a high activation-energy barrier between the single macroion state and the oligomer state. Another possibility is that due to the small size of the $\mathbf{U_{28}}$, thermal fluctuation may have a stronger influence on the stability of the macroion/counterion ion pairings in solution, so the ΔG between the single POMs and the blackberries becomes smaller. From our previous studies based on POM macroions (size 2–5 nm), both enthalpy and entropy might contribute to the blackberry formation.[20] Herein, with smaller $\mathbf{U_{28}}$ ions, the contribution from the entropy change might be particularly lower.

Under extreme conditions when the activation energy barrier is high enough or the ΔG is small enough, it is reasonable to assume that POMs can no longer form blackberries in solution.

Self-recognition between two U_{28} clusters in solution

Both Rb**Na**$\mathbf{U_{28}}$ and Cs**K**$\mathbf{U_{28}}$ were found to be able to form blackberry structures in solution with additional electrolytes, however, with different lag phases and sizes (Figure 4A). Prior to this, we observed more rapid exchange between external and internal alkali cations if the cations inside are smaller, or in other words, larger internal alkali cations exit the capsule slower.[18] This was nicely confirmed by the conductivity measurements for both $\mathbf{U_{28}}$ clusters in 2.44×10^{-3} M KOH solution (see the Supporting Information). Rb**Na**$\mathbf{U_{28}}$ has a higher conductance than Cs**K**$\mathbf{U_{28}}$ in 2.44×10^{-3} M KOH solution, which indicates more counterions are released from the Rb**Na**$\mathbf{U_{28}}$ cluster. Interestingly, we noticed that the lag time for Cs**K**$\mathbf{U_{28}}$ is longer than that for Rb**Na**$\mathbf{U_{28}}$ in KOH solution. At first glance, this is contrary to our prior observation that lower charge density of the cluster provides better conditions for blackberry formation than higher charge density. This can be explained by considering all the counterions as templating counterions and linking counterions. Templating counterions stay inside the cluster, therefore, they do not directly contribute to the counterion induced attraction force between two adjacent $\mathbf{U_{28}}$ clusters; instead, they only tune the charge density of the cluster.

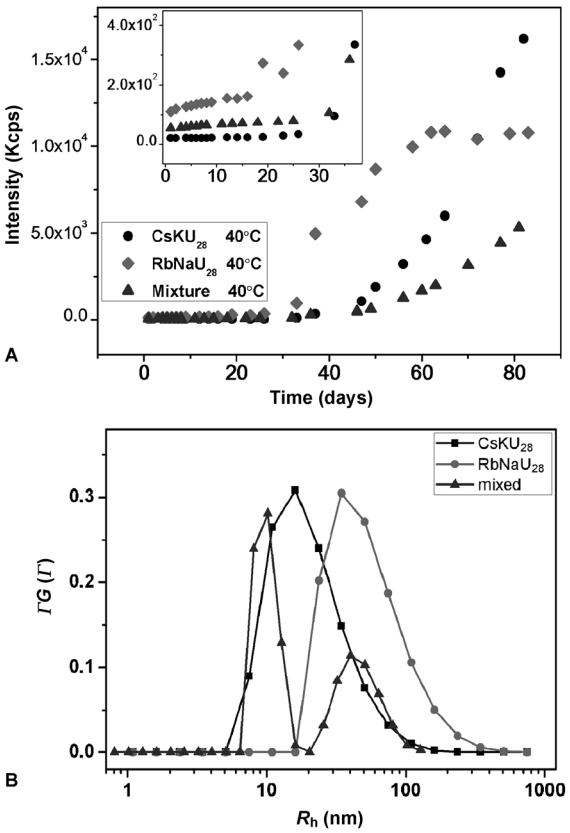

Figure 4. A) Total scattered intensity change with time for three different $\mathbf{U_{28}}$ samples in the 0.05 mol L^{-1} KOH solution at 40 °C. Black dots represent a 0.5 mg mL^{-1} CsK$\mathbf{U_{28}}$ sample; diamonds represent a 0.42 mg mL^{-1} (4.31×10^{-5} mol L^{-1}) RbNa$\mathbf{U_{28}}$ sample; and triangles represent a mixture of the two $\mathbf{U_{28}}$ clusters with half concentration of each. B) R_h distribution plot of three $\mathbf{U_{28}}$ samples in 0.05 mol L^{-1} KOH solution at 40 °C, recorded by DLS at a scattering angle of 45° on the 50th day after sample preparation. Black squares: 4.31×10^{-5} mol L^{-1} RbNa$\mathbf{U_{28}}$; dots: 4.31×10^{-5} mol L^{-1} CsK$\mathbf{U_{28}}$; and triangles: their 1:1 mixture.

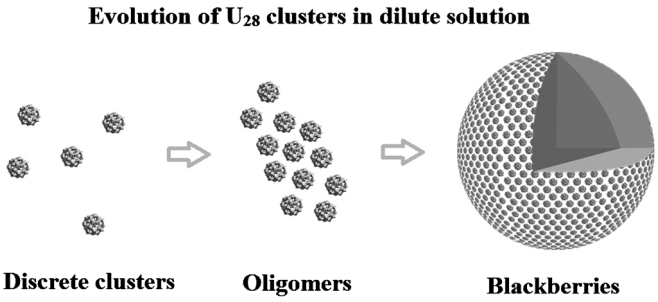

Scheme 2. Evolvement of $\mathbf{U_{28}}$ clusters in dilute electrolyte solutions.

On the other hand, the linking counterions are those external counterions and partially released internal counterions, which can serve as linkage to "connect" two $\mathbf{U_{28}}$ clusters together to form metastable ion pairings. Because the RbNa$\mathbf{U_{28}}$ clusters release more internal counterions into solution than the CsK$\mathbf{U_{28}}$ clusters do, the counterion-induced attraction between the RbNa$\mathbf{U_{28}}$ clusters will be stronger than that of the CsK$\mathbf{U_{28}}$ clusters at the initial stages of blackberry assembly. Therefore, the RbNa$\mathbf{U_{28}}$ clusters have a relatively short lag phase than the CsK$\mathbf{U_{28}}$ clusters do in solution. (Scheme 2)

Furthermore, repeated ^{23}Na and ^{133}Cs NMR analyses of the solutions, in which blackberry assembly had been observed, utilizing different spectrometers (both at SNL and Lehigh) and in both quartz and glass NMR tubes suggested that the majority of the templating alkali cations had indeed exited the capsules into the solution. Although we could easily observe these encapsulated NMR-active templating cations in freshly prepared $\mathbf{U_{28}}$ solutions, it was not possible to observe them in the solutions, in which blackberry assembly had occurred. One may argue that the exiting of these alkali cations from the capsules results in clusters with even higher negative-charge density than the nominal formulation provided in Table 1. However, we can suggest that the net result of these alkalis being released from the capsules actually enhances blackberry formation by the following arguments.

Because solutions of $\mathbf{U_{28}}$ have an alkaline self-buffering pH, and neither the peroxide nor oxo ligands tend to protonate, we believe this is due to replacement of the alkalis that exit the clusters with H_3O^+, because it is not reasonable to expect a void to remain within the capsule. This means that the overall charge of the capsules is not necessarily significantly reduced, although we cannot accurately measure this at the current stage.

Release of the majority of the alkalis into solution from the capsule (enhanced by heating), particularly the large alkalis, such as Rb^+ and Cs^+, provides extra alkalis to link the clusters together in the blackberry assembly. The solid-state structures show that the larger alkali cations, such as Cs^+, find ideal binding sites outside of the capsule: the pentagonal face in particular. There is a reason to assume this binding site also remains favorable in solution: prior studies on other cluster-cation systems have shown that alkali-polyanion association observed in solid-state structures may also persist in solution.[4b]

An interesting question is when the two $\mathbf{U_{28}}$ clusters are 1:1 mixed together in solution, will they form individual blackberry structures or mixed ones, that is, whether they can self-recognize with each other, similar to what was observed for the $\{Mo_{72}Fe_{30}\}$ and $\{Mo_{72}Cr_{30}\}$ systems.[1b] We tested this idea by mixing the two $\mathbf{U_{28}}$ clusters together and compared the mixed solution with solutions of individual $\mathbf{U_{28}}$ clusters. As shown in Figure 4 A, although the initial time-resolved scattered-intensity curve for the mixture stays between the two individual clusters, which is not a surprise because the initial scattered intensity is proportional to the concentration of single $\mathbf{U_{28}}$ clusters in solution, the self-assembly process in the mixed sample solution is much slower than the individual cases due to the lower cluster concentration. We have shown in Figure S2 in the Supporting Information that the higher $\mathbf{U_{28}}$ concentration tends to have a faster increment in the scattered intensity (i.e., a faster self-assembly process). If the two $\mathbf{U_{28}}$ clusters form mixed blackberries, the mixed solution should have the same speed of self-assembly, because the two individual ones (then a time-resolved scattered-intensity curve with the same slope as the two individual solutions). As shown in Figure 4 A, the different formation speed indicates that these two $\mathbf{U_{28}}$ are not

identical to each other due to the different surface-charge densities, and they could self-recognize during the oligomer-formation step. Further evidence comes from the R_h distribution plot (Figure 4B), recorded by DLS at a scattering angle of 45° on the 50th day after the sample preparation. In three $\mathbf{U_{28}}$ samples (RbNa$\mathbf{U_{28}}$, CsK$\mathbf{U_{28}}$, and their 1:1 mixture) in 0.05 mol L^{-1} KOH solution at 40 °C, two individual peaks with size being about 10 and 40 nm were found in the mixture sample, which can be attributed to the two different sized assemblies from CsK$\mathbf{U_{28}}$ (ca. 18 nm) and RbNa$\mathbf{U_{28}}$ (ca. 53 nm).

Conclusion

The small actinyl cluster of $\mathbf{U_{28}}$ has shown different self-assembly behaviors than large polyoxomolybdates or polyoxovanadates in solution to date. It is the smallest macroion that can form blackberry structures in solution. The small macroionic size might result in much more complex self-assembly process including an extended lag phase, which is sensitive to the counterion type, counterion concentration, and temperature during the self-assembly process of the $\mathbf{U_{28}}$ clusters. Moreover, the $\mathbf{U_{28}}$ clusters do not directly form blackberry structures, but do form through some intermediate states. The mixture of two populations of $\mathbf{U_{28}}$ clusters, differing in their internal templating cations, can recognize each other and form individual blackberry structures in solution. These unique behaviors stem from the high surface-charge density and the small size of the $\mathbf{U_{28}}$, as well as the unique aspect of internal cations, together with external cations, which would affect the activation energy barrier and the stability of macroion/counterion ion pairing. Herein, we have documented the first example of blackberry formation of the smallest metal–oxo clusters, as well as the first macroion assembly of uranyl clusters. Because the macroion self-assembly processes is intimately tied to anion/cation pairing in solution, this study adds to the now-growing database of knowledge of the ever-important relationship between anions and cations in aqueous systems.

Experimental Section

Synthesis of U_{28} clusters

Methods to form CsK$\mathbf{U_{28}}$ and RbNa$\mathbf{U_{28}}$ have been reported before.[17a,18]

Preparation of sample solutions

Solutions of $\mathbf{U_{28}}$ were prepared by dissolving $\mathbf{U_{28}}$ cluster salts into aqueous electrolyte solutions, for example, 0.05 mol L^{-1} of KOH. The final concentrations of $\mathbf{U_{28}}$ are between 0.1–5.0 mg mL^{-1}. Dust contamination was eliminated by filtering the solutions through 0.2 μm Millipore filter units into precleaned glass vials for light-scattering measurements.

Laser-light scattering

Both dynamic light scattering (DLS) and static light scatting (SLS) techniques were used to monitor the $\mathbf{U_{28}}$ solutions. A Brookhaven Instruments Inc. laser-light-scattering spectrometer, equipped with a 532 nm diode-pumped solid-state (DPSS) laser and a BI-9000AT multichannel digital correlator was used for all experiments. The SLS was performed over a broad range of scattering angles from 30 to 130°, with 2° intervals. The radius of gyration (R_g) of the solute particles was directly calculated from the software provided by Brookhaven Instruments Inc. For DLS measurements, the intensity/intensity time-correlation functions were analyzed by the constrained regularized (CONTIN) method to ascertain the average hydrodynamic radius (R_h) of the large assemblies. The average apparent translational diffusion coefficient, D_{app}, was determined from the normalized distribution function of the characteristic line width, Γ(G). The hydrodynamic radius R_h is converted from D through the Stokes–Einstein Equation [Eq. (2)]:

$$R = k_B T / 6\pi\eta D \qquad (2)$$

in which k_B is the Boltzmann constant and η is the viscosity of the solvent at temperature T. The particle size distribution in solution was obtained by plotting ΓG(Γ) versus R_h, with $\Gamma_i G_i$ (Γ_i) being proportional to the angular-dependent scattered intensity of particle i having an apparent hydrodynamic radius $R_{h,i}$. The temperature in the sample chamber was controlled to within ±0.1 °C. Further detailed information about SLS and DLS can be found in our previous publications.[1a]

Transmission electron microscopy (TEM)

Samples for electron-microscopy characterization were prepared by pipetting 5 μL of the sample solution onto a carbon-coated TEM grid. The TEM samples were left under ambient conditions for several hours until the solvent completely evaporated. Bright-field (BF) TEM imaging was performed on a JEOL 2000FX transmission electron microscope with an accelerating voltage of 200 kV.

Acknowledgements

T.L. acknowledges support from the NSF (CHE1305756), Lehigh University, and The University of Akron. This work was supported as part of the Materials Science of Actinides, an Energy Frontier Research Centre funded by the Department of Energy, Office of Science, Office of Basic Energy Sciences under award number DE-SC0001089.

Keywords: actinides · laser-light scattering · macroions · polyoxometalates · self-assembly

[1] a) T. Liu, E. Diemann, H. Li, A. W. M. Dress, A. Muller, *Nature* **2003**, *426*, 59–62; b) T. Liu, M. L. K. Langston, D. Li, J. M. Pigga, C. Pichon, A. M. Todea, A. Müller, *Science* **2011**, *331*, 1590–1592; c) R. N. Biboum, F. Doungmene, B. Keita, P. de Oliveira, L. Nadjo, B. Lepoittevin, P. Roger, F. Brisset, P. Mialane, A. Dolbecq, I. M. Mbomekalle, C. Pichon, P. Yin, T. Liu, R. Contant, *J. Mater. Chem.* **2012**, *22*, 319–323.

[2] a) T. Liu, *Langmuir* **2010**, *26*, 9202–9213; b) A. Oleinikova, H. Weingärtner, M. Chaplin, E. Diemann, H. Bögge, A. Müller, *ChemPhysChem* **2007**, *8*, 646–649; c) E. Fratini, A. Faraone, A. M. Todea, P. Baglioni, *Inorg. Chim. Acta* **2010**, *363*, 4234–4239.

[3] a) P. Yin, D. Li, T. Liu, *Chem. Soc. Rev.* **2012**, *41*, 7368–7383; b) D. Li, W. Zhou, K. Landskron, S. Sato, C. J. Kiely, M. Fujita, T. Liu, *Angew. Chem.* **2011**, *123*, 5288–5293; *Angew. Chem. Int. Ed.* **2011**, *50*, 5182–5187.

[4] a) P. Linse, V. Lobaskin, *J. Chem. Phys.* **2000**, *112*, 3917; b) M. R. Antonio, M. Nyman, T. M. Anderson, *Angew. Chem.* **2009**, *121*, 6252–6256; *Angew. Chem. Int. Ed.* **2009**, *48*, 6136–6140; *Angew. Chem.* **2009**, *121*, 6252–6256.

[5] a) N. Ise, I. S. Sogami, *Structure Formation in Solution: Ionic Polymers and Colloidal Particles*, Springer, Heidelberg, **2005**; b) X. López, C. Nieto-Draghi, C. Bo, J. B. Avalos, J. M. Poblet, *J. Phys. Chem. A* **2005**, *109*, 1216 – 1222.

[6] a) W. M. Gelbart, R. F. Bruinsma, P. A. Pincus, V. A. Parsegian, *Phys. Today* **2000**, *53*, 38; b) R. Das, T. T. Mills, L. W. Kwok, G. S. Maskel, I. S. Millett, S. Doniach, K. D. Finkelstein, D. Herschlag, L. Pollack, *Phys. Rev. Lett.* **2003**, *90*, 188103; c) S. A. Pabit, X. Qiu, J. S. Lamb, L. Li, S. P. Meisburger, L. Pollack, *Nucleic Acids Res.* **2009**, *37*, 3887 – 3896; d) T. E. Angelini, R. Golestanian, R. H. Coridan, J. C. Butler, A. Beraud, M. Krisch, H. Sinn, K. S. Schweizer, G. C. L. Wong, *Proc. Natl. Acad. Sci. USA* **2006**, *103*, 7962 – 7967.

[7] G. Liu, T. Liu, S. S. Mal, U. Kortz, *J. Am. Chem. Soc.* **2006**, *128*, 10103 – 10110.

[8] a) P. C. Burns, R. C. Ewing, A. Navrotsky, *Science* **2012**, *335*, 1184 – 1188; b) W. Briner, *Int. J. Environ. Res. Public Health* **2010**, *7*, 303 – 313; c) D. Brugge, V. Buchner, *Rev. Environ. Health* **2011**, *26*, 231 – 249; d) W. J. Hartsock, J. D. Cohen, D. J. Segal, *Chem. Res. Toxicol.* **2007**, *20*, 784 – 789.

[9] a) W. Runde, *Los Alamos Sci.* **2000**, *26*, 392 – 411; b) K. H. Williams, J. R. Bargar, J. R. Lloyd, D. R. Lovley, *Curr. Opin. Biotechnol.* **2013**, *24*; in press; c) S. Yan, B. Hua, Z. Bao, J. Yang, C. Liu, B. Deng, *Environ. Sci. Technol.* **2010**, *44*, 7783 – 7789.

[10] P. C. Burns, *Can. Mineral.* **2005**, *43*, 1839 – 1894.

[11] M. Nyman, P. C. Burns, *Chem. Soc. Rev.* **2012**, *41*, 7354 – 7367.

[12] P. Miró, S. Pierrefixe, M. Gicquel, A. Gil, C. Bo, *J. Am. Chem. Soc.* **2010**, *132*, 17787 – 17794.

[13] a) P. C. Burns, *Mineral. Mag.* **2011**, *75*, 1 – 25; b) J. Qiu, P. C. Burns, *Chem. Rev.* **2013**, *113*, 1097 – 1120; c) P. O. Adelani, M. Ozga, C. M. Wallace, J. Qiu, J. E. S. Szymanowski, G. E. Sigmon, P. C. Burns, *Inorg. Chem.* **2013**, *52*, 7673 – 7679; d) P. O. Adelani, G. E. Sigmon, P. C. Burns, *Inorg. Chem.* **2013**, *52*, 6245 – 6247.

[14] C. R. Armstrong, M. Nyman, T. Shvareva, G. E. Sigmon, P. C. Burns, A. Navrotsky, *Proc. Natl. Acad. Sci. USA* **2012**, *109*, 1874 – 1877.

[15] J. Qiu, J. Ling, A. Sui, J. E. S. Szymanowski, A. Simonetti, P. C. Burns, *J. Am. Chem. Soc.* **2012**, *134*, 1810 – 1816.

[16] P. C. Burns, K.-A. Kubatko, G. Sigmon, B. J. Fryer, J. E. Gagnon, M. R. Antonio, L. Soderholm, *Angew. Chem.* **2005**, *117*, 2173 – 2177; *Angew. Chem. Int. Ed.* **2005**, *44*, 2135 – 2139; *Angew. Chem.* **2005**, *117*, 2173 – 2177.

[17] a) M. Nyman, M. A. Rodriguez, T. M. Alam, *Eur. J. Inorg. Chem.* **2011**, 2197 – 2205; b) A. Gil, D. Karhánek, P. Miró, M. R. Antonio, M. Nyman, C. Bo, *Chem. Eur. J.* **2012**, *18*, 8340 – 8346.

[18] M. Nyman, T. M. Alam, *J. Am. Chem. Soc.* **2012**, *134*, 20131 – 20138.

[19] a) J. Zhang, D. Li, G. Liu, K. J. Glover, T. Liu, *J. Am. Chem. Soc.* **2009**, *131*, 15152 – 15159; b) T. Liu, *J. Am. Chem. Soc.* **2003**, *125*, 312 – 313; c) T. Liu, *J. Am. Chem. Soc.* **2002**, *124*, 10942 – 10943.

[20] G. Liu, T. Liu, *Langmuir* **2005**, *21*, 2713 – 2720.

[21] J. M. Pigga, J. A. Teprovich, R. A. Flowers, M. R. Antonio, T. Liu, *Langmuir* **2010**, *26*, 9449 – 9456.

Received: August 19, 2013
Published online on January 8, 2014